Toward high resolution images with SQUID-based ultra-low field magnetic resonance imaging

Michelle Espy[1], *Member, IEEE,* Per Magnelind, Andrei Matlashov, Shaun Newman, Algis Urbaitis, Petr Volegov

***Abstract*— Magnetic resonance imaging (MRI) is the state-of-the art clinical method for imaging soft-tissue anatomy. Because signal scales with the applied magnetic field, the overwhelming trend in MRI has been to high magnetic fields, typically 1.5 or 3 T. However, there has been recent interest in ultra-low field (ULF) MRI using 10-100 μT magnetic fields. At ULF there are opportunities for novel imaging applications such as MRI combined with magnetoencephalography (MEG) in a single device, imaging through or in the presence of metal, and enhanced spin-lattice tissue contrast. Loss in signal is mitigated by sensitive detectors such as superconducting quantum interference devices (SQUIDs) and sample pre-polarization, typically from 10-100 mT. There have been several proof-of-concept demonstrations based on this approach. However, ULF MRI image quality still suffers from one or more of the following disadvantages compared to HF MRI: lower signal-to-noise ratio, poor spatial resolution, and longer imaging time. Here we present recent progress toward "clinically relevant" ULF MRI parameters: voxel SNR > 10, voxel size < 2×2×4 mm^3. Data and simulations from a single channel system are presented and discussed.**

***Index Terms*— SQUID MRI, ULF MRI, MEG, SQUID array.**

I. Introduction

Magnetic Resonance Imaging (MRI) is the state-of-the art clinical method for imaging soft-tissue anatomy. The fundamental principle behind MRI is to magnetize (polarize) a sample with non-zero nuclear spin in a large magnetic field. This magnetization can then be manipulated by subsequent application of magnetic fields to produce a measurable signal at a unique (Larmor) frequency ω_0, which is specific to the measurement (readout) magnetic field B_0 and the type of nuclei,

$$\omega_0 = \gamma B_0 , \qquad (1)$$

where γ is the gyromagnetic ratio.

In traditional high field (HF) anatomical MRI, which we define as that using a polarization field > 1 Tesla, the sample is typically the spin ½ protons found in water inside the body, γ = 42.6 MHz/T. The subject is placed inside a large, highly uniform (ppm), fixed strength, usually superconducting magnet of 1.5 or 3 T. The polarization, B_p, and measurement, B_m, magnetic field are the same, with a proton Larmor frequency of ~ 64 – 128 MHz.

Practically, the higher the polarizing magnetic field achieved the better, in terms of signal. This is because the sample equilibrium magnetization, M_{eq}, scales as

$$M_{eq} = \frac{N\hbar^2\gamma^2 I(I+1)B_p}{3k_B T} , \qquad (2)$$

where N is the number of spins in a voxel, γ is the gyromagnetic ratio (rad/T-sec form), I is the spin number, k_B is the Boltzmann constant (1.381×10^{-23} J/K) and T is the temperature. The increased signal can be used for faster acquisition and higher resolution images.

An additional motivation for high magnetic fields is that the performance of Faraday coils used as detectors in HF MRI, increases with magnetic field strength [1]. Thus trying to perform conventional MRI at lower magnetic field strengths results in a penalty in acquired signal that scales as ~ ω_0^2.

However, there remain numerous MRI applications where high field is not an option. Examples include performing MRI simultaneously with brain imaging methods such as magnetoencephalography (MEG) [2] which is simply not possible in a HF MRI machine due to the large mismatch in magnetic fields; MRI in the presence of metal [3,4] where heating or distortions increase with applied fields; or imaging applications where a large and expensive magnet might be impractical.

In the early 2000's John Clarke's group at UC Berkeley significantly advanced the concept of SQUID-based MRI at ultra-low fields (ULF), with readout magnetic fields as low as at 1 – 100 μT [5]. The approach relied on pulsed pre-polarization [6] at higher fields (0.01 - 0.1 T) to increase signal.

Numerous applications of SQUID-based ULF MRI using this approach have been demonstrated by us and others, including imaging the human brain [2,7,8]. However, ULF MRI image quality still suffers from the following disadvantages compared to HF MRI: lower signal-to-noise ratio (SNR), poor spatial resolution, and longer imaging times. These arise not just from low polarization but also from unique challenges presented by instrumentation, tissue contrast, and other realities of the ULF regime. It is worth mentioning that ULF MRI simply cannot compete with HF MRI in terms of image quality on its own. One should pursue the ULF regime only when the benefits outweigh the drawbacks. In this paper we will discuss many of the

Manuscript received October 9, 2012. This work was supported by the Los Alamos National Laboratory, Laboratory Directed Research and Development Office. The authors thank Samitaur Medical Technologies for support in acquisition of the high resolution phantom images.

All authors are with Los Alamos National Laboratory, Los Alamos, USA. Corresponding author: Michelle Espy (phone: 505-412-8705; fax: 505-665-4507, e-mail: espy@lanl.gov.).

challenges of imaging in the ULF regime, in the context of our own quest to improve the quality of ULF MRI images for brain imaging.

II. Imaging Basics

A. General MRI considerations

In general, the physical principles used for ULF MRI are very similar to those used for traditional MRI. The primary differences with ULF include: 1) less signal and lower bandwidth; 2) different requirements for generation and manipulation of magnetic fields (which enable novel pulse sequences, but also introduce new demands); 3) differences in detector technology (i.e. the SQUID vs. Faraday coil); and 4) differences in T_1 contrast. Here we briefly review some fundamental concepts in MRI that will be helpful in highlighting the differences between HF and ULF approaches discussed in the next section. An excellent and far more complete description of conventional MRI can be found in Ref. [9].

The principal aim of all MRI is to spatially encode the NMR properties (e.g. T_1, T_2, or spin density) underlying the information available in the images. In MRI such encoding is based on the fact that the Larmor frequency over the sample depends on the spatial profile of the applied magnetic field over the sample, see (1).

If we wish to spatially encode we intentionally apply a magnetic field gradient $\mathbf{G}(t)$ (assumed to be a linear gradient for these discussions) that causes the local Larmor frequency to vary in a known way, such that

$$\omega(\mathbf{r},t) = \omega_0 + \gamma \mathbf{G}(t)\cdot\mathbf{r} \qquad (3)$$

Neglecting relaxation effects for the moment, the NMR signal $S(t)$ in a single voxel (dV) will be

$$dS(t) \propto \rho(\mathbf{r}) \exp(i\int_0^t \omega(\mathbf{r},t')dt')dV\ , \qquad (4)$$

where $\rho(\mathbf{r})$ is the spin density, and $\omega(\mathbf{r},t')$ is the Larmor frequency over the sample during the measurement. In (4) we assume that the primary Larmor frequency established by B_0 does not vary with time or position *during* the signal measurement time. However, the ability to manipulate the measurement field in strength and orientation *between* measurements to extract different information from the image is a key feature of the ULF MRI approach that typically differs from high field approaches.

The signal from the sample becomes

$$S(t) = \exp(i\varphi(t))\iiint q(\mathbf{r})\exp(i\int_0^t \gamma G(t')\cdot\mathbf{r}dt')\,, \qquad (5)$$

where $q(\mathbf{r})$ is the contrasted spin density that is proportional to the local spin density $\rho(\mathbf{r})$ and, when a suitable preparatory sequence is used, the relaxation times $T_1(\mathbf{r})$ and $T_2(\mathbf{r})$, and on the diffusion coefficient $D(\mathbf{r})$. The integral over the main Larmor frequency is expressed as a time-varying phase $\int_0^t \omega_0(t')dt' = \varphi(t)$.

In the approach of (5) we are assuming that the signal is obtained from the entire sample. We next introduce the concept of the reciprocal space vector [10,11]

$$\mathbf{k} \equiv \frac{\gamma}{2\pi}\int_0^t \mathbf{G}(t')dt' \qquad (6)$$

and following the outline in Callaghan [9] we re-write (5) as

$$\mathrm{S}(\mathbf{k}) = \exp(\mathrm{i}\varphi(\mathrm{t}))\iiint q(\mathbf{r})\exp(\mathrm{i}2\pi\mathbf{k}\cdot\mathbf{r})dV \qquad (7)$$

and

$$\mathrm{q}(\mathbf{r}) = \exp(\mathrm{i}\varphi(\mathrm{t}))\iiint S(\mathbf{k})\exp(\text{-}\mathrm{i}2\pi\mathbf{k}\cdot\mathbf{r})d^3k\ . \qquad (8)$$

Equations (7) and (8) are a Fourier transform pair showing that the signal and spin density are mutually conjugate. This is a fundamental formulation underlying MRI. In MRI the pulse sequence is typically thought of as the trajectory through *k*-space, where the gradient is like the velocity term. How we apply the gradients will determine the course [12].

B. Imaging at ULF: The challenges

Thus far the published ULF MRI images of the brain [2,7,8] have had voxel dimensions of 3-4 mm at best. The imaging times have been long, > 60 minutes, and averaging (of 4 or more images) has been required to improve the SNR to > 10. While the definition of "clinically relevant" is subjective (i.e. it is relevant if there is a clinical application in which it is used), it is generally accepted that an image of the brain ought to be able to resolve key anatomical features (e.g. cerebellum). Somewhere around a voxel size of 2 × 2 × 4 mm^3 and SNR ≥ 10 is where images meet these criteria. HF MRI images of the brain with 1 × 1 × 3 mm^3 and SNR ~ 100 are routinely achieved in < 20 minutes. While we reiterate that the point of ULF MRI is not to compete with HF, we might consider meeting these basic criteria as an imaging goal.

What issues have thus far prevented ULF MRI from meeting these basic criteria? The first is the obvious problem with low magnetization (hence SNR) illustrated in (2). The second is related to the low strength of the imaging gradients; they limit bandwidth and dictate long acquisition times on par with relaxation times (which are typically shorter at ULF). Thus at the same time that we are required to acquire for longer, we are running out of signal. The third is related to the requirement for very low noise signal generation, which has thus far kept pulse sequences rather inefficient.

To help frame the discussion, in Fig. 1 we present a schematic of the ULF MRI system which was used to acquire our first brain images, as well as the images presented later in this paper. B_p are the magnetic field coils to generate the sample magnetization, in this example along the *x*-axis. B_m denotes the measurement magnetic field coils, along the *z*-axis. The additional $G_{x,y,z}$ coils are for gradient encoding in the B_z/dx,y,z directions respectively. In HF MRI there is a single fixed field providing both B_p and B_m, typically provided by a large superconducting magnet. In ULF MRI the field generation is typically produced by simple electromagnets.

This allows for different field orientations and strengths provided by separate B_p and B_m coils. Fig. 2 shows the Fourier Imaging pulse sequence used.

Low magnetization seems to have an obvious solution; build more powerful pulsed pre-polarization fields. In some ways ULF MRI has advantages, the B_p does not have to be highly homogeneous, which simplifies the magnet requirements. But it is not trivial to make a pulsed field at > 50 mT. The coil will experience heating, the energy must be removed, and the proximity of a large amount of conductor near the SQUIDs can introduce noise. Use of appropriate materials, such as Litz wire can reduce this. Further, the coil can be physically disconnected with a switch. We have built pulsed B_p coils using resistive copper cooled by Fluorinert at room temperature, and also liquid nitrogen (LN) [13]. The LN coil has the benefit of 7x lower resistance, but requires the complexity of an additional cryostat. Both designs are still rather large (weighing hundreds of pounds). Neither design has operated in excess of ~ 100 mT. Recently a group in Finland has shown a self-shielded [14] pulsed superconducting coil [8] for ULF MRI, integrated directly into the cryostat with the SQUIDs. However, in that work the superconducting wire appeared to become magnetized if too high a current (> 12 A) were applied, producing gradients that influenced the image quality, and presently limiting B_p to < 24 mT.

While the optimal conductor choice for B_p remains to be seen, the use of a self-shielded design as proposed in [14] is likely critical. This is because a very serious problem, especially for combined MEG/MRI applications, is that the pulsing fields can cause huge transients in nearby conducting materials. The magnetically shielded room required for MEG can support transients with components that can persist for hundreds of msec [15]. The fields from such transients are hard to de-convolve from the MEG [8]. Even when not measuring MEG, these transients can impose a long dead-time between pulsing and acquisition while waiting for them to decay. As we mentioned, if T_1 is short (as is often the case at ULF) this means valuable signal is being lost while we wait. An adiabatic removal of B_p ($dB_p/dt << \gamma B_m^2$) can help further minimize transients. However, given these issues, to generate

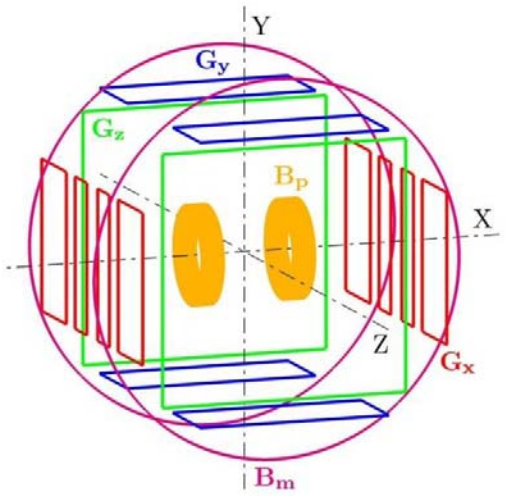

Figure 1. Schematic of ULF MRI field generation coil system.

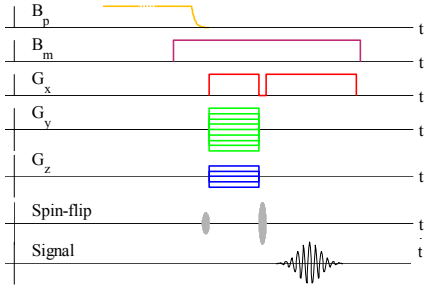

Figure 2. ULF MRI pulse sequence.

and remove a field > 100 mT over a large volume like the head is non-trivial.

For our discussion of the issues presented by low gradients we remind the reader of a few additional imaging concepts. Equations (7) and (8) define the relationship between the spatial and frequency domain by a Fourier transform pair. From the Nyquist theorem it follows that for any real signal (using the x-direction as an example)

$$\Delta x = 1/2W_x = 1/2\left(k_{x,\max} - k_{x,\min}\right), \qquad (9)$$

and

$$\Delta k_x = 1/2L_x = 1/2\left(x_{\max} - x_{\min}\right), \qquad (10)$$

where W_x is the extent of the image in the k-space domain and L_x is the extent of the image in the spatial domain.

What (9) and (10) illustrate is that the extent of the image in the spatial domain or field-of-view, FOV, is related to the resolution in the k-space domain. And conversely, the spatial resolution is related to the extent of the image in the k-space domain.

Assuming that the gradient does not change over the acquisition time (6) becomes (along x, which is our readout direction)

$$k_{x,\max} - k_{x,\min} = (2\pi)^{-1}\gamma G_x t_a, \qquad (11)$$

where t_a describes the time during which the gradient is switched on, the acquisition time. Thus we can describe the spatial resolution as

$$\Delta x = 2\pi(2\gamma G_x t_a)^{-1} \qquad (12)$$

Spatial resolution in other directions is arrived at similarly. What is immediately obvious from this equation is that in order to improve the spatial resolution, one either has to make the gradient or the acquisition (or encoding) time large. But in ULF MRI the gradients are not large. They are typically on the order of 10^{-4} T/m, about 100x smaller than high field MRI. Thus one has to have acquisition times proportionally longer. Further, one cannot just turn up the gradient strength due to problems with concomitant gradients (see for example [16]). The low magnetic fields also present bandwidth limitations. From the Nyquist theorem sampling should be at

$$t_a = \frac{N}{2\Delta\omega} \qquad (13)$$

For an object 10 cm across, (using the gyromagnetic ratio ~ 42.6 MHz/T for protons and typical 10^{-2} T/m gradients found in HF MRI) we have a frequency spread of about 42 kHz across. If we take a typical 100 encoding steps to image we have $\Delta\omega$ = 420 Hz, and an acquisition time of ~ 1.2 ms per

step. In a ULF MRI system the 100-fold lower gradients again lead us to commensurately longer acquisition, i.e. 120 ms. But at ULF the T_1 and T_2 times for many interesting tissues are approximately this long [17], so we are also running out of signal at the same time. To increase the gradient strength would widen the frequency spread across the object, but with a low central frequency, we are then measuring in a challenging low frequency regime.

Now let us briefly return to the discussion of field-of-view (FOV). FOV is related to the spatial resolution by the number of steps as

$$L_x = (N_x - 1)\Delta x \,. \qquad (14).$$

Given the longer time to take each step compared to HF MRI, one very important time-saving approach is to use multiple sensor arrays to reduce the steps required. This enables imaging acceleration methods [18]. The ULF MRI method lends itself quite naturally to a multiple sensor approach [19]. In ULF MRI combined with MEG, a dense sensor array is available anyway. MEG-like dense sensor arrays have been used even in HF MRI and shown significant acceleration [20].

Finally, it is worth mentioning that the Fourier Imaging sequence shown in Fig. 2 is extremely inefficient for ULF MRI. Significant time is spent encoding, while signal is relaxing away. Also only one echo per pre-polarization excitation is typically possible, further increasing imaging time. But such an approach is expedient because in this case only the minimal magnetic fields (B_m and G_x) need to be on during readout, minimizing noise coupled to the SQUIDs.

III. Results of a Single Channel System

To determine the feasibility of achieving the desired metrics for image resolution (SNR > 10, voxel size < 2×2×4 mm^3) we next describe a modeling and experimental effort to evaluate the performance of a single channel ULF MRI system.

A. System Simulation

Fig. 3 shows the simulation set-up of the 7-channel ULF MRI system we used to perform the ULF MRI experiments described below. The properties of the system have been described elsewhere [21]. The inset shows the actual acrylic phantom, filled with water, used for the work. The holes are 3 mm in diameter, 6 mm deep, and spaced 5 mm apart. The simulation code was written in MATLAB, based on the Biot-Savart-LaPlace formulation of magnetostatics and the reciprocity principle. Such an approach, while not general, allows for computationally efficient modeling of our ULF MRI system. In Fig. 4 we show the results of a simulation with the parameters listed in the second column of Table 1. For this image we assumed a noise of 1 fT/√(Hz).

B. Imaging a water phantom

Fig. 5 shows an experimentally measured ULF MRI of the acrylic phantom filled with water. The pre-polarization field was ~ 100 mT, the readout field 94 μT. The voxel size is 0.9 × 0.9 × 6 mm^3. An SNR of ~ 12 was achieved in a single 8 minute scan. Data were taken with the system shown in Fig. 1

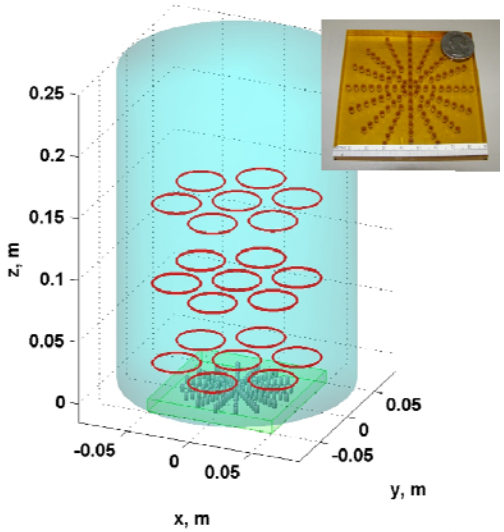

Figure 3. System simulation showing locations of gradiometer coils (circles), and the position of the phantom. Inset shows the acrylic phantom, with holes 3 mm in diameter and 6 mm deep.

and pulse sequence in Fig. 2. Only the central channel of a 7 SQUID gradiometer array was used as a surface-coil detector with a FOV of ~ 5 cm. The noise of this channel had been experimentally measured to be ~ 1.2 fT/√(Hz), in the presence of un-energized MRI coils. Additional imaging parameters are summarized in the third column of Table 1.

The image shown in Fig. 5 is consistent with our model for the signal from water (not shown) but only when we assume a noise level of 3 fT/√(Hz). This additional noise arises from the fact that when the MRI coils are active, there is added noise that must be accounted for.

C. Imaging tissue

Because the image shown in Fig. 5 was based on water, the relaxation time was long (~ 3 sec). Thus rather long encoding and acquisition times of 76 and 150 ms, respectively, were possible. However, the relaxation times of tissue are on this order (100 – 200 ms) at ULF and thus one critical requirement towards imaging a biological object is slightly increased gradients for shorter times.

New gradient coils were fabricated allowing us to increase from ~8 Hz/mm to ~18 Hz/mm. Also, new gradient coil current supplies with water-cooled current limiting resistors

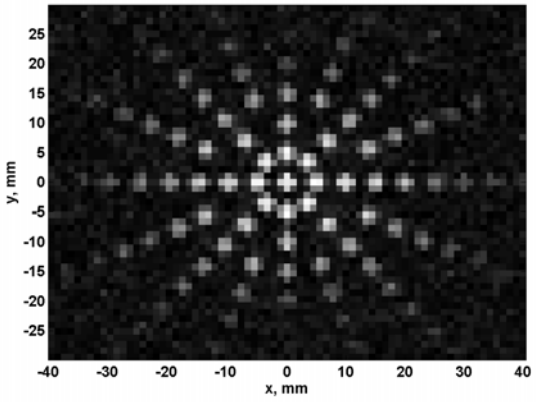

Figure 4. Simulation of the phantom. T_2 was set to ~ 150 ms to mimic the properties of tissue. The imaging parameters are listed in Table 1.

Table 1. Parameters for measured and simulated images.

	Fig. 4	**Fig. 5**	**Fig. 6**	**Fig. 7**
T_2 [s]	0.150	3	0.150	0.150
t_g encoding [ms]	25	76	25	25
Voxel size [mm^3]	1.1×1.1×6	0.9×0.9×6	0.9×0.9×6	0.9×0.9×6
N_x (read-out	73	89	89	89
N_z (phase steps)	55	81	81	81
N_{avg}	1	1	10	10
t_a acquisition	50	150	50	50
$G_{x,z}$ [Hz/mm]	18	8	18	18
B_p [mT]	100	100	75	50
SNR_{image} [a.u.]	27	12	16	17

were developed to drive the four coils.

Using this new system, we were able to reduce the encoding and acquisition time to 25 and 50 ms, respectively. However, shortly after we acquired the image in Fig. 5, we had a significant failure in our B_p amplifiers which also appeared to compromise the B_p coil. Interestingly, after recovery from the failure we also observed a ~ 3-fold increase in noise in the imaging system. We hypothesize that this excess noise was a result of magnetization of some component of the cryostat or gradiometer probes. The noise was resolved by a complete thermal cycle of the system. But it highlights an interesting problem when using pulsed pre-polarization especially as we drive towards higher fields: the potential for magnetization of components must be considered, yet many ULF MRI systems rely on cryostats that are re-purposed from other approaches (e.g. MEG) and never intended to experience such conditions. At the time of this writing we were only able to recover to a pre-polarization field of 75 mT, limited by the noise increase.

To mimic the properties of real tissue, we doped the water in the phantom with $CuSO_4$ to reduce the relaxation time to ~0.15 s. The resulting image is shown in Fig. 6. The imaging parameters are given in the fourth column of Table 1.

The image in Fig. 6 appears of similar quality, compared to Fig. 5 (our other experimentally acquired image). However, the image is for 10 averages. To fully understand if the differences between the images in Figs 5 and 6 are consistent, we first introduce a method for comparing images via the concept of device SNR (or imaging efficiency) [22].

The acquired signals and reconstructed image, for a single voxel, are linked by

$$SNR_{voxel} = \sqrt{N_x N_z N_{\text{avg}}}\left(S_0 \big/ \sigma_s\right), \qquad (15)$$

where $N_{x,y,z}$ is the number of pixels (readout and phase encode steps, we neglect the N_y step here for a 2D image). S_0 is the signal in the time domain (for example a sine-wave from precessing magnetization, neglecting relaxation). S_0 is proportional to the voxel volume, V, and the magnetization (magnetic field)

$$S_0 \approx V \cdot \chi_0 \approx V \cdot B_{\text{p}}. \qquad (16)$$

The noise in the acquisition bandwidth, σ_s, can be expressed

$$\sigma_s = \sqrt{\sigma_n^2 \cdot N_x \big/ t_a}, \qquad (17)$$

where σ_n is system noise, N_x is the number of readout steps, and t_a the acquisition time. The relation N_x/t_a is the acquisition bandwidth.

Putting Equations (15), (16), and (17) together we find that we can describe the SNR of a device as

$$\left(B_P \big/ \sqrt{\sigma_n^2}\right) \propto SNR_{voxel} \big/ dV \cdot \sqrt{N_{\text{avg}} N_z t_a}. \qquad (18)$$

Using the numbers in Table 1, we would expect the SNR of the image in Fig. 6 to be ~ 16.4. This is in excellent agreement with our observed SNR of 16.

When we model the expected image at 75 mT and with 3 fT/√(Hz), it is quite similar to the image in Fig. 6. This image is shown in Fig. 7. Here we find that our result is entirely consistent with the model. Ten averages and a longer than desired scan time of 40 minutes were both required to achieve our SNR and spatial resolution goals at B_p = 75 mT and 3 fT/√(Hz) noise. The result is consistent with scaling from Fig. 5 using the concept of device SNR, or through modeling.

IV. Towards a "High Resolution" Image

To achieve the desired image properties it appears 100 mT

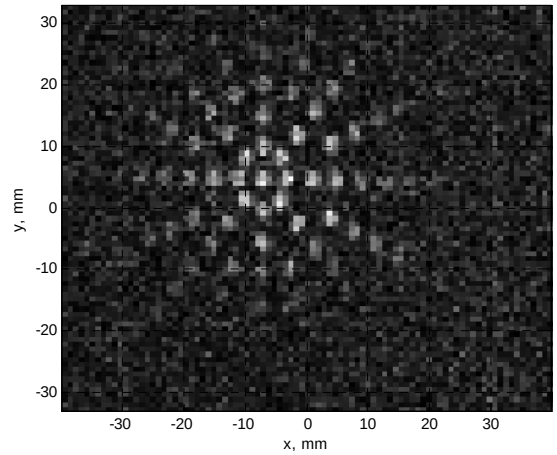

Figure 5. ULF MRI measured for water at 94 μT. The imaging parameters are listed in Table 1.

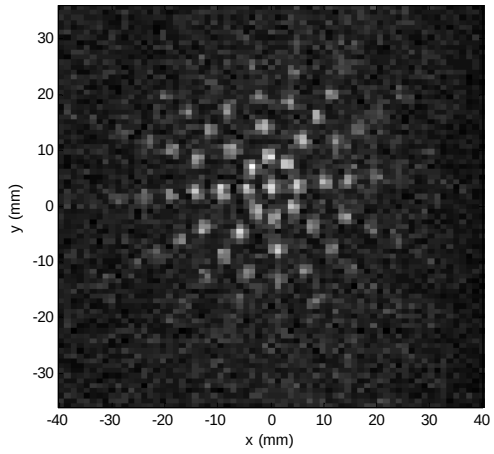

Figure 6. ULF MRI measured for $CuSO_4$ doped de-ionized water. T_2 was ~ 150 ms. The image is an average of 10 scans.

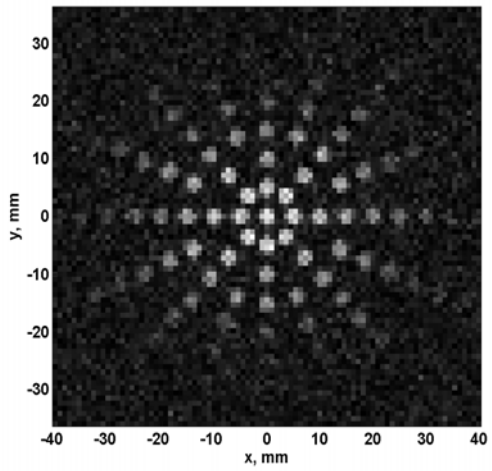

Figure 7. Simulation of the phantom with T_2 ~ 150 ms, 50 mT polarization, and 3 fT/√(Hz). Imaging parameters are listed in Table 1.

and 1 fT/√(Hz) are minimal requirements. These will be challenging to obtain over a large field of view such as the human head. The short T_2 times of tissue will be a confound given the requirement for longer acquisitions. We often assume that the SQUID noise is as measured in zero field. This fails to take into account the inevitable noise increase associated with the MRI fields, or the influence of stray magnetic fields on the image quality. Further, ULF MRI often relies on instrumentation not originally intended for the application, such as cryostats designed for MEG. This can only add to the noise. Additionally, very simple instrumentation (i.e. batteries) are a work-around to the issue of noise introduced by the imaging coils, but will greatly limit the pulse sequences available.

V. Discussion and Conclusions

ULF MRI will not compete with HF MRI in terms of image quality as defined by SNR and spatial resolution, for a given scan time. It is also clear that with the exception of the contrast, which may need to be measured; almost every aspect of a ULF MRI system can, and should be modeled. With realistic values for polarization and noise, the image quality can be determined *a priori*. We hope our discussion in this paper will motivate the further use of such realistic modeling.

Although there are challenges, we remain optimistic that there are applications where the unique contrast or capabilities of ULF MRI remain distinct and advantageous. If it is possible to achieve the requisite polarization and noise, reasonable image quality is possible. There is a fundamental reality that the images are going to take longer. However, the use of multiple sensors lends itself especially to ULF MRI (coupling issues from parallel arrays that arise in HF MRI are not a problem since the sensors are not highly tuned coils). The sensor array approach is capable of performing image acceleration using the spatial sensitivity of the array instead of encoding steps. This is likely the only way to reduce the long imaging times.

Acknowledgment

This work was supported in part by the Los Alamos National Laboratory LDRD #20100097DR. The authors thank Samitaur Medical Technologies for support in acquisition of the high resolution phantom images.

References

[1] W. Myers et al., "Calculated signal-to-noise ratio of MRI detected with SQUIDs and Faraday detectors in fields from 10 micro Tesla to 1.5 Tesla," J. Magn. Reson., vol. 186, issue 2, pp. 182–192, 2006.

[2] V. S. Zotev et al., "Microtesla MRI of the human brain combined with MEG," J. Magn. Reson., vol. 194 (1), pp. 115–120, 2008

[3] M. Mößle et al., "SQUID-Detected Microtesla MRI in the Presence of Metal," J. Magn. Reson., vol. 179, pp. 146-151, 2006.

[4] A.N. Matlachov et al.,"SQUID detected NMR in microtesla magnetic fields," J. Magn. Reson., vol. 170, pp. 1–7, 2004.

[5] J. Clarke, M. Hatridge, and M. Mößle, "SQUID-Detected Magnetic Resonance Imaging in Microtesla Fields", Annu. Rev. Biomed. Eng., vol. 9, pp. 389–413, 2007.

[6] A. Macovski, S. Conolly, "Novel approaches to low cost MRI," Magn. Reson. Med., vol. 30, pp. 221–230, 1993.

[7] P. E. Magnelind et al.,"Co-Registration of Interleaved MEG and ULF MRI Using a 7 Channel Low-Tc SQUID System," IEEE Trans. Appl. Supercond., vol. 21, issue 3, pt. 1, pp. 456–460, 2011.

[8] P. T. Vesanen et al.,"Hybrid ultra-low-field MRI and MEG system based on a commercial whole-head neuromagnetometer," Magn. Reson. Med., in press.

[9] P.T. Callaghan, Principles of Nuclear Magnetic Resonance Microscopy, Oxford University Press Inc., New York, 1993.

[10] S. Ljunggren, "A simple graphical representation of Fourier-based imaging methods," J. Magn. Reson., vol. 54 (2), pp. 338–343, 1983.

[11]D. Twieg D, "The k-trajectory formulation of the NMR imaging process with applications in analysis and synthesis of imaging methods," Medical Physics, vol. 10 (5), pp. 610–621, 1983.

[12] http://www.ebyte.it/library/educards/mri/K-SpaceMRI.html

[13] J. R. Sims et al., "Low-Noise Pulsed Pre-Polarization Magnet Systems for Ultra-Low Field NMR," IEEE Trans. Appl. Supercond., vol. 20 (3), pp. 752–755, 2010.

[14] J. O. Nieminen et al.,"Avoiding eddy-current problems in ultra-low-field MRI with self-shielded polarizing coils," J. Magn. Reson., vol. 212, 154–160, 2011.

[15] P. Vesanen et al.,"The spatial and temporal distortion of magnetic fields applied inside a magnetically shielded room," IEEE Transactions on Magnetics, vol. 48 (1), pp. 53–61, 2012.

[16] P. L. Volegov et al.,"On concomitant gradients in low-field MRI," J. Mag. Res., vol. 175 (1), pp. 103–113, 2005.

[17] V. S. Zotev et al., "SQUID-based microtesla MRI for in vivo relaxometry of the human brain," IEEE Trans. Appl. Supercond., vol. 19, issue 3, pt.1, pp. 823–826, 2009.

[18] K. P. Pruessmann et al.,"SENSE: Sensitivity encoding for fast MRI," Mag. Reson. Med., vol. 42, issue 5, pp. 952–962, 1999.

[19] V. Zotev et al.,"Parallel MRI at microtesla fields," J. Magn. Reson., vol. 192, issue 2, pp. 197–208, 2008.

[20] F-H. Lin et al., "Dynamic magnetic resonance inverse imaging of human brain function," Magn. Reson. Medicine, vol. 56 (4), pp. 787–802, 2006.

[21] V. S. Zotev et al.,"SQUID-based instrumentation for ultra-low-field MRI," Supercond. Sci. Technol., vol. 20 (11), pp. S367–S373, 2007.

[22] E. M. Haacke et al.,"Chapter 15: Signal, Contrast, and Noise", in Magnetic Resonance Imaging; Physical Principles and Sequence Design, John Wiley and Sons, 1999, pp. 348–349, 1999.